J Membrane Biol (2012) 245:509–520
DOI 10.1007/s00232-012-9432-8

ORIGINAL ARTICLES

In Vivo Muscle Electroporation Threshold Determination: Realistic Numerical Models and In Vivo Experiments

Selma Čorović · Lluis M. Mir · Damijan Miklavčič

Received: 20 December 2011 / Accepted: 30 April 2012 / Published online: 24 May 2012

Abstract In vivo electroporation is used as an effective technique for delivery of therapeutic agents such as chemotherapeutic drugs or DNA into target tissue cells for different biomedical purposes. In order to successfully electroporate a target tissue, it is essential to know the local electric field distribution produced by an application of electroporation voltage pulses. In this study three-dimensional finite element models were built in order to analyze local electric field distribution and corresponding tissue conductivity changes in rat muscle electroporated either transcutaneously or directly (i.e., two-plate electrodes were placed either on the skin or directly on the skeletal muscle after removing the skin). Numerical calculations of electroporation thresholds and conductivity changes in skin and muscle were validated with in vivo measurements. Our model of muscle with skin also confirms the in vivo findings of previous studies that electroporation "breaks" the skin barrier when the applied voltage is above 50 V.

S. Čorović · D. Miklavčič (✉)
Faculty of Electrical Engineering, University of Ljubljana, Trzaska 25, 1000 Ljubljana, Slovenia
e-mail: damijan.miklavcic@fe.uni-lj.si

S. Čorović
e-mail: selma.corovic@fe.uni-lj.si

S. Čorović · L. M. Mir
UMR 8203 CNRS, Laboratoire de Vectorologie et Thérapeutiques Anticancéreuses, Institute Gustave-Roussy, 114 rue Edouard Vaillant, 94805, Villejuif Cedex, France
e-mail: luis.mir@igr.fr

S. Čorović · L. M. Mir
UMR 8203, University of Paris-Sud XI, Paris, France

Keywords Muscle electroporation · Skin electroporation · Electric field · Numerical model · Electrochemotherapy · Gene therapy · Vaccination

Introduction

Tissue electroporation (also termed "electropermeabilization") is a transient electrical increase of cell membrane permeability by means of local delivery of short and sufficiently intense voltage pulses (i.e., electroporation pulses) to the target tissue cells via properly selected electrodes (Miklavcic et al. 2000). In vivo electroporation is used as an effective technique for the delivery of a variety of therapeutic agents, such as chemotherapeutic drugs, DNA or other molecules which in normal conditions do not cross the cell membrane, into many different target tissue cells (Mir et al. 1995; Prud'homme et al. 2006). Skeletal muscle tissue is one of the most promising tissues for DNA delivery by electroporation for either local or systemic gene therapy and gene vaccination (Mir et al. 1999; Mathiesen 1999; Tevz et al. 2008; Hojman et al. 2009). Investigating in vivo muscle tissue electroporation is relevant to both clinical electrochemotherapy (Marty et al. 2006; Edhemovic et al. 2011) and transdermal drug delivery (Denet et al. 2004) for providing knowledge on the sensitivity of underlying muscle tissue to the electroporation procedure (Zupanic et al. 2007; Mali et al. 2008), as well as in various physiological and developmental studies (Breton and Mir 2011).

The key parameter in effective tissue electroporation is local electric field distribution, E (the symbol E refers to the magnitude of the vector of electric field intensity), established within the treated tissue due to the delivered electroporation pulses. Target tissue cells can be electroporated

in a reversible and safe way only within the tissue regions subjected to a local electric field (E) of a magnitude comprised between reversible (E_{rev}) and irreversible (E_{irrev}) electroporation thresholds (Miklavcic et al. 1998). The magnitude of E can be controlled by carefully choosing electroporation pulse amplitude and electrode configuration, given that the electroporation thresholds E_{rev} and E_{irrev} and the tissue's electrical and geometrical properties are known (Zupanic et al. 2008; Corovic et al. 2008; Kos et al. 2010). An important prerequisite for the determination of E_{rev} and E_{irrev} thresholds is the visualization of the local electric field distribution with numerical calculations in realistic tissue models which are validated with corresponding experimental observations and, thus, take into account realistic geometric and electrical properties of the tissues to be modeled (Miklavcic et al. 1998; Sel et al. 2005; Corovic et al. 2010). Since the electroporation thresholds (and thus the induced transmembrane potentials at these thresholds) are related to the cell size, density and orientation with respect to the electric field and to the parameters of the electroporation pulses, they have to be determined for each cell and tissue type (Pavlin et al. 2002; Valic et al. 2003). Theory and experiments also showed that when the cells are electroporated, their electrical properties change due to the increase in the cell membrane's conductivity, which is reflected in the bulk conductivity increase (Pavlin and Miklavcic 2003). It was previously suggested that tissue conductivity changes, as an indicator of the tissue electroporation level, can also be assessed by in vivo measurements of changes in tissue conductance (Davalos et al. 2002, 2004; Ivorra et al. 2009) and of the total current flowing through the treated tissues (Cukjati et al. 2007).

The protocols for in vivo muscle electroporation, for muscle electroporated either transcutaneously or directly (i.e., without skin), were established based on the ratio of the amplitude of applied electroporation pulses relative to the distance between the electrodes. Very few studies investigated the local electric field distribution in the muscle and its surrounding tissues (Gehl et al. 1999; Pavselj et al. 2005; Corovic et al. 2010). In most of the studies on skin electroporation, a pronounced change in skin resistance indicating skin electroporation was reported to occur at voltages above 50 V (Prausnitz et al. 1993; Pliquett et al. 1995).

The aim of our study was to develop realistic numerical models in order to investigate the E_{rev} and E_{irrev} thresholds and the electroporation process between these thresholds in skeletal muscle tissue electroporated either transcutaneously or directly. We numerically and experimentally investigated the local electric field distribution as well as the geometric and electrical properties of skin and muscle tissue electroporated separately and of muscle electroporated through the skin. We observed an influence on electroporation efficiency in muscle tissue due to the presence of skin.

We built three separate realistic numerical models of skinfold, muscle and muscle with skin. Changes in electrical properties resulting from electroporation were modeled by determining the functional dependence of tissue conductivity, σ (S/m), on local electric distribution (E) above the reversible electroporation threshold (E_{rev}) in each of the examined tissues. Using finite element methods, we calculated local electric field distribution and total electric current at voltages of equal amplitudes as the electroporation pulses that were applied in in vivo experiments.

In order to validate the realistic numerical models that we developed in this study, we mathematically interpreted the data collected during an extensive in vivo study on the response of the skin, muscle and muscle with skin to the electroporation pulses (Cukjati et al. 2007). We compared the results of our numerical simulations to the in vivo total current measurement and ^{51}CrEDTA-uptake results. From the numerical models validated on the experimentally obtained results we determined electroporation parameters such as reversible and irreversible electroporation threshold values, E_{rev} and E_{irrev}; the initial tissue conductivity (before the electroporation pulses were applied), σ_0; the conductivity of the same tissue modified due to the electroporation, σ_1; and the functional dependence of tissue conductivity on local electric field distribution, $\sigma(E)$, between the thresholds.

The same electroporation threshold values were found, as expected, for both muscle electroporated transcutaneously and directly since the electroporation threshold is a property of the tissue and cannot be affected by neighboring tissues. However, in order to electrically overcome the skin barrier, a higher voltage between the electrodes (i.e., amplitude of electroporation pulses applied) was required when the muscle was electroporated through the skin in contrast to electroporation directly on the muscle.

Methods

In Vivo Experiments

Animals

Female Wistar rats purchased from Janvier (Le Genest Saint Isle, France) were used for the experiments. Rats were anesthetized by intraperitoneal administration of ketamine (100 mg/kg; Panpharma, Frankfurt, Germany) and xylazine (10 mg/kg; Bayer, Leverkusen, Germany). Animals were handled according to recommended good

practices and standard institutional ethics rules for animal experimentation (UKCCCR 1998).

^{51}Cr-EDTA

To determine the electropermeabilization level of skin and muscle tissue when applying electroporation pulses directly or transcutaneously in vivo, we performed the quantitative uptake method using ^{51}Cr-EDTA as the indicator (Gehl and Mir 1999; Cukjati et al. 2007). Animals were given 200 µl of ^{51}Cr-EDTA (Amersham, Aylesbury, UK) with a specific activity of 3.7 MBq/ml intravenously 5 min before delivery of the electric pulses. The injected ^{51}Cr-EDTA distributes freely in the vascular and extracellular compartments and can enter the intracellular compartments only if access is provided (e.g., by electroporation). Animals were killed 24 h after injection, and tissues exposed to electric pulses were removed, weighed and counted in a Cobra 5002 gamma counter (Packard Instrument, Meriden, CT). Net ^{51}Cr-EDTA uptake as a result of electropermeabilization was calculated as the measured activity (converted to nanomoles of ^{51}Cr-EDTA) per gram of tissue exposed to the electric pulses. ^{51}Cr-EDTA-uptake values were then used to calculate mean values of uptake (±SEM) as a function of the ratio of the applied voltage to the electrodes' distance in the rat skeletal muscle electroporated transcutaneously or directly.

Electroporation Protocol

Electroporation pulses consisted of a train of eight square-wave and 100-µs-long pulses, delivered at a repetition frequency of 1 Hz. In all experiments the electric pulses were generated by a PS 15 electropulse generator (Jouan, St. Herblain, France) and delivered to the tissue through two parallel plate stainless-steel electrodes. The electrode dimensions used in our experiments are shown in Fig. 1a. The following three experiments were carried out: electroporation of skin tissue only (a skinfold was formed and placed between the electrodes, as shown in Fig. 1b), direct muscle electroporation (the skin was previously removed and the plate electrodes were placed directly on the muscle surface, Fig. 1c) and transcutaneous muscle electroporation (Fig. 1d). Electrodes were positioned on the tissue so that the electric field was perpendicular to the muscle fibers. We treated the triceps brachii muscle of the hind limb and the gastrocnemius medialis muscle of the forelimb. Electrodes were separated by 5.7 mm for the muscles electroporated directly and transcutaneously and by 2.8 mm for electroporation of the skinfold. Good contact between the electrodes and tissue was assured by the use of a gel (ultrasound transmission gel EKO-GEL; Camina, Egna, Italy). During the electroporation pulse delivery, the applied voltage and the actual current delivered were monitored and collected using a digital oscilloscope (Waverunner; LeCroy, Chestnut Ridge, NY).

The input used for in vivo experiments was the amplitude of the delivered electric pulses to the tissue. The output from the experiment was the measured electric current and the measured ^{51}CrEDTA absorption.

Numerical Modeling

Experimentally treated tissues were mathematically modeled as passive volume conductors in a quasi-stationary electric current field. Electric field distribution (i.e., local electric field, E [V/cm]) in the tissue models caused by electroporation pulses was determined by numerically solving Laplace's equation:

$$-\nabla\,(\sigma\cdot\nabla\varphi)=0 \qquad (1)$$

where σ and φ represent tissue conductivity (S/m) and electric potential (V), respectively. The calculated E in our models was used to calculate threshold values for

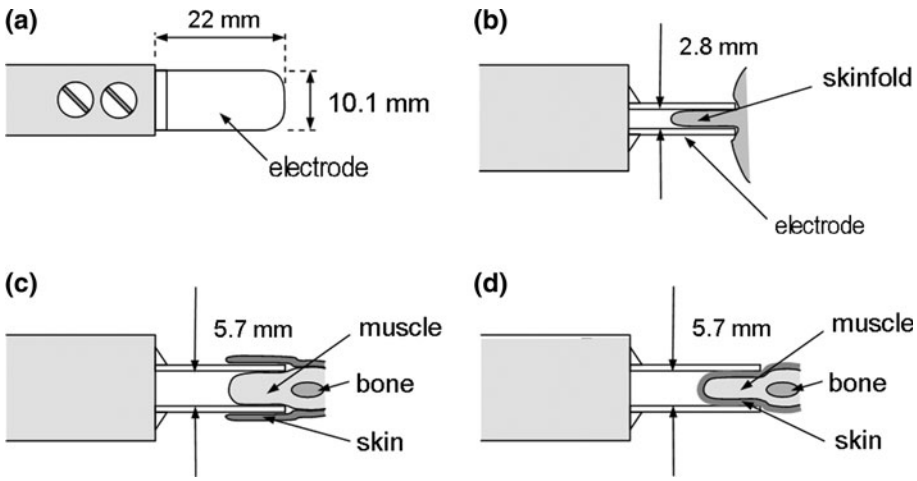

Fig. 1 Electrode dimensions used in experiments (**a**) and geometry of the measurement setup for skinfold electroporation (**b**) and muscle electroporated directly (**c**) and transcutaneously (**d**)

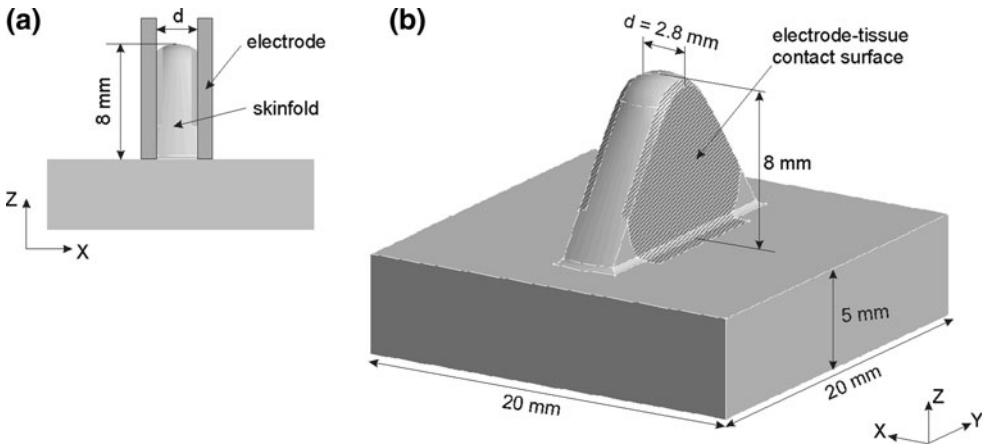

Fig. 2 Geometry of the skinfold finite element model in the *zx* cross-sectional plane (**a**) and in 3D (**b**). Patterned region represents the contact surface between the electrode and tissue geometry (i.e., electrode—tissue contact surface)

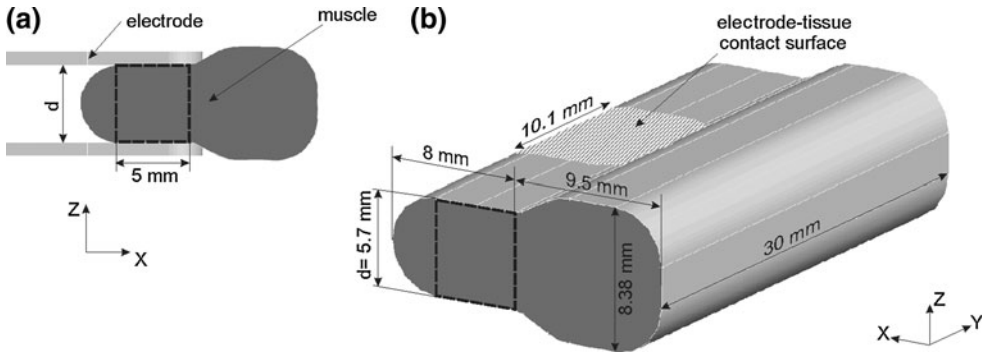

Fig. 3 Geometry of the muscle tissue finite element model (electroporated directly) in the *zx* cross-sectional plane (**a**) and in 3D (**b**). Patterned region represents the contact surface between the electrode and tissue geometry (i.e., electrode—tissue contact surface)

reversible (E_{rev}) and irreversible (E_{irrev}) tissue electroporation. Total electric current flowing through the 3D modeled tissues was then calculated according to Ohm's law. In the first stage of numerical modeling we built 3D models of the skinfold (Fig. 2), muscle tissue electroporated directly (Fig. 3) and muscle tissue electroporated transcutaneously (Fig. 4) using the commercial software package EMAS (Ansoft, Canonsburg, PA). Taking into account the fact that electric field distribution and total electric current flowing through the tissue depend strongly on the tissue geometry, we designed the geometry of our numerical models as accurately as possible. Applied voltage, U (V, model input), was modeled as Dirichlet's boundary condition on the contact surface between electrode and tissue geometry. For the model input values we used the amplitudes of the electroporation pulses applied in vivo (Cukjati et al. 2007). We mathematically separated the conductive segment from its surroundings by applying Neuman's boundary condition ($J_n = 0$, where J_n is the normal electric current density [A/m^2]) on all outer boundaries of the model.

Results of the calculated model outputs (total electric current, I, and local electric field distribution, E) were controlled for numerical errors by increasing the size of our model and increasing the mesh density until the electric insulation condition and error due to meshing irregularities

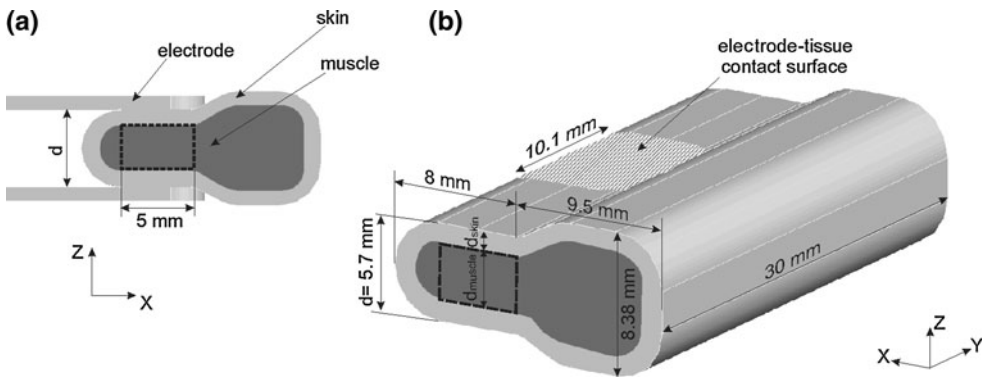

Fig. 4 Geometry of muscle electroporated transcutaneously in the *zx* cross-sectional plane (**a**) and in 3D (**b**). Patterned region represents the contact surface between the electrode and tissue geometry (i.e., electrode—tissue contact surface)

were insignificant—a further increase in domain size or mesh density only increased the computation time; however, the results changed by <0.5 %. The resulting models—mesh of skinfold, muscle and muscle electroporated transcutaneously—consisted of 4173, 7546 and 10074 tetrahedral finite elements, respectively.

Electric Properties of the Modeled Tissues and Electroporation Process Modeling

In our numerical models, ohmic tissue behavior was analyzed (i.e., skin and muscle conductivities, σ). Before applying electroporation pulses or if the amplitude of the applied electroporation pulses was too low to produce a local electric field above the reversible electroporation threshold ($E < E_{rev}$), the tissues were modeled as linear conductors with linear current–voltage, I (U), relationships due to the constant tissue conductivities. The initial prepulse values of conductivities (σ_0 corresponding to the $E < E_{rev}$ condition) used in numerical models were selected from the available literature (Miklavcic et al. 2006). Muscle tissue was considered an anisotropic conductor, being more conductive along the muscle fibers in the y axis compared to the two other perpendicular x and z axes (Table 1), while skin tissue was considered isotropic and homogeneous. Since the skin tissue was not the primary target of our investigation, different layers of skin were not modeled; thus, an average value for conductivity was assigned to skin tissues in our models (Table 1). Namely, large differences in skin layer geometries would unnecessarily increase the computational time of numerical simulations while not contributing to the accuracy of the electric field distribution in the muscle tissue (Pavselj et al. 2005).

If the local electric field in the tissues exceeded the E_{rev} value, the tissue electric properties changed (i.e., tissue conductivity increased due to the electroporation process). During the application of electroporation pulses, tissue conductivity increased according to the functional dependence of the tissue conductivity on the local electric field distribution, $\sigma(E)$, which in our study described the dynamics of the electroporation process. This subsequently resulted in a nonlinear dependence of the electric current as a function of the applied voltage $I(U)$. Thus, due to the change of σ, we detected the threshold electroporation E_{rev} as a result of the deviation of $I(U)$ from the linear relationship $I = U/R$ (where R [ohm] is tissue electric resistance).

The tissue electroporation dynamics were modeled based on the sequential permeabilization model proposed by Sel et al. 2005, where changes in tissue conductivity were used as an indicator of tissue permeabilization. For this purpose a sequence analysis subprogram (as an extension of EMAS) was developed to model the dynamics of electroporation as a sequence of static FEM models. The subprogram was developed so as to avoid the oscillations in electric conductivity and to allow only the local electric field intensity to change due to the conductivity increase. In each static description in the dynamic sequence of tissue changes, tissue conductivity was determined based on the electric field distribution from the previous step in the sequence, as described in the following equation:

$$\sigma(k) = f[E(k-1)] \tag{2}$$

where k stands for the number of static FEM steps in the sequence.

Model input is the applied voltage, U, and model outputs are the electric field distribution, E, and total electric current, I, in each specific sequence step, k. The modeled tissue behavior during the electroporation pulse delivery is illustrated in Fig. 5. In our models we took into account only the current measurement (I_k) at the end of the pulses, which corresponds to the value of the current calculated in the first sequence (I_5 in $k = 5$) in which the $\sigma(E)$ in our models stabilized. The output current from I_5 was then compared to the measured current at the end of the eighth pulse (i.e., output from the in vivo corresponding experiment).

The increase in electrical current I from I_0 to I_k simulates the tissue response in each discrete interval k during

Table 1 Electroporation parameters σ_o, σ_1, E_{rev} and E_{irrev} calculated in single models of skinfold and muscle tissue

Tissue	σ_0 (S/m)	σ_1 (S/m)	E_{rev} (V/cm)	E_{irrev} (V/cm)
Skin	0.008	20 σ_o	480	1,050
Muscle	x and y axes	3.5 σ_o	240	450
	0.135			
	z axis[a]			
	0.75			

[a] Numerical calculations showed that varying the factor σ_1/σ_o in z axis did not significantly change the $I(U)$ characteristic

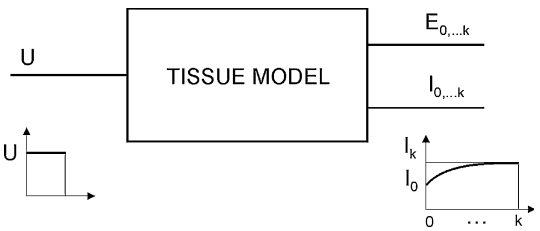

Fig. 5 Modeled tissue behavior during electroporation pulse delivery, where U is the amplitude of the electroporation pulses delivered to the tissues, E is the electric field strength, I is the total electric current calculated in each sequence step and k is the number of steps in the sequence corresponding to the duration of the electroporation pulses

the delivery of the electroporation pulses U to the tissue (due to the functional dependence of σ on the electric field distribution E). If electroporation does not occur, σ remains constant; thus, $I = I_0$. The sequence analysis subprogram gives us a choice of five different $\sigma(E)$ relationships given by Eqs. 3–7.

$$\sigma(E) = \begin{cases} \sigma_0, & E < E_{\text{rev}} \\ \sigma_1, & E \geq E_{\text{rev}} \end{cases} \tag{3}$$

$$\sigma(E) = \begin{cases} \sigma_0, & E < E_{\text{rev}} \\ \frac{\sigma_1 - \sigma_0}{E_{\text{irrev}} - E_{\text{rev}}} \cdot (E - E_{\text{rev}}) + \sigma_0, & E_{\text{rev}} \leq E < E_{\text{irrev}} \\ \sigma_1, & E \geq E_{\text{irrev}} \end{cases} \tag{4}$$

$$\sigma(E) = \begin{cases} \sigma_0, & E < E_{\text{rev}} \\ A \cdot \left(1 - \exp\left(\frac{E - E_{\text{rev}}}{B}\right)\right) + \sigma_0, & E_{\text{rev}} \leq E < E_{\text{irrev}} \\ \sigma_1, & E \geq E_{\text{irrev}} \end{cases} \tag{5}$$

$$\sigma(E) = \begin{cases} \sigma_0, & E < E_{\text{rev}} \\ A \cdot \left(\exp\left(\frac{E - E_{\text{irrev}}}{B}\right) - 1\right) + \sigma_1, & E_{\text{rev}} \leq E < E_{\text{irrev}} \\ \sigma_1, & E \geq E_{\text{irrev}} \end{cases} \tag{6}$$

$$\sigma(E) = \begin{cases} \sigma_0, & E < E_{rev} \\ \sigma_0 + \frac{\sigma_1 - \sigma_0}{\left(1 + \exp\left(-\frac{E - a}{B}\right)\right)}, & E_{\text{rev}} \leq E < E_{\text{irrev}} \\ \sigma_1, & E \geq E_{\text{irrev}} \end{cases} \tag{7}$$

where $A = \frac{\sigma_0 - \sigma_1}{\exp\left(\frac{E_{\text{rev}} - E_{\text{irrev}}}{B}\right) - 1}$ and $a = \frac{E_{\text{rev}} + E_{\text{irrev}}}{2}$

Parameters σ_0 and σ_1 represent the initial prepulse tissue conductivity and the conductivity of electroporated tissue, respectively; parameters E_{rev} and E_{irrev} stand for reversible and irreversible electroporation thresholds of the local electric field, respectively; and parameter B defines the shape of the exponential and sigmoid functions.

Single-Tissue Models—Skin and Muscle Tissue Models

First, we modeled the electroporation process in each of the tissue models separately: skinfold (Fig. 2) and muscle tissue (Fig. 3). The same values of applied voltages in vivo were applied to the contact surfaces of the single muscle and skin models as model inputs. A comparison of the current as a function of the voltage $I(U)$ to the measured ones in vivo was used to determine which of the functional dependencies given by Eqs. 3–7 best described the dynamics of the electroporation process in each of the tissues analyzed. Namely, in order to tune our single-tissue models for in vivo electroporation of skinfold (Fig. 1b) and for direct in vivo muscle electroporation (Fig. 1c) measurement, we varied different functional relationships (step [Eq. 3], exponential [Eqs. 4, 5], linear [Eq. 6], and sigmoidal [Eq. 7] functions) with different reversible and irreversible electroporation threshold values until good agreement between $I(U)$ obtained numerically and the $I(U)$ characteristic measured in vivo was established.

From the resulting numerical models, we collected the initial prepulse tissue conductivity, σ_0; the conductivity of the electroporated tissues, σ_1; and the $\sigma(E)$ relationships between the reversible and irreversible threshold values, E_{rev} and E_{irrev} (with the corresponding parameters a, A and B).

Complete Muscle Tissue Model—Model of Muscle Electroporated Transcutaneously

The $\sigma(E)$ relationships with E_{rev} and E_{irrev} obtained from single models of the skin (Fig. 2) and muscle (Fig. 3) were applied to the skin and muscle composing the complete model (model of muscle electroporated transcutaneously) (Fig. 4). The same values of voltages of transcutaneous muscle electroporation in vivo (Fig. 1d) were applied to the contact surfaces of the complete muscle with skin model (Fig. 4). In order to tune the intricate muscle model with the transcutaneously electroporated muscle in vivo, we also varied the thickness of the skin (d_{skin} parameter in Fig. 4) until the $I(U)$ relationship matched the measured one. In such a way we numerically detected the complete muscle tissue geometry that corresponded to realistic muscle with a skin layer treated in our experiments in vivo, and we validated the model parameters σ_0, the conductivity of σ_1 and the $\sigma(E)$ relationships with E_{rev} and E_{irrev} collected from the single-tissue electroporation modeling. In order to compare the conductivity change and geometry of skin layer numerically found in the intricate muscle model to the data from the published literature, we also calculated the complete muscle model resistance, R, for each of the voltages applied.

Analysis of the Influence of Skin Presence on Muscle Electroporation

In order to analyze the influence of the skin layer on muscle electroporation, we compared the local electric field distribution in muscle electroporated directly (Fig. 3) with the local electric field distribution obtained in the muscle only, inside the intricate muscle model with skin (Fig. 4). For this purpose, we wrote a program with Matlab7a to calculate the average local electric field at the end of the electroporation process (i.e., the final sequence FEM model for each voltage applied).

The average electric field intensities were calculated in the volumes between two plate electrodes (the regions between electrodes marked with a dashed square in Figs. 3, 4), where the local electric field (E) was the most homogeneous (i.e., equal to the applied voltage to the inter-electrode distance ratio [$E = U/d$]). In this way we numerically removed the skin layer from the complete

muscle model with skin shown in Fig. 4. The numerical results of E in the muscle from the complete model were then compared to the numerical results of E calculated in the numerical model of the directly electroporated muscle.

Results and Discussion

The aims of our study were to develop realistic numerical models in order to investigate the electroporation process in skeletal muscle tissue electroporated directly and transcutaneously and to examine the influence of the presence of the skin on the electroporation process in muscle tissue. For this purpose, we numerically and experimentally investigated the local electric field and the geometric and electrical properties of electroporated skinfold and muscle tissue electroporated directly and transcutaneously. Numerical calculations of the local electric field were performed by means of the finite element method and sequential modeling of tissue electroporation (Sel et al. 2005), taking into account realistic geometries and electrical properties of the examined tissues. Local electric field distribution was experimentally assessed by measurement of the total current and of ^{51}CrEDTA uptake in vivo. The 3D realistic models of skinfold and muscle electroporated directly and transcutaneously were then developed (based on good agreement between numerical calculations and experimental observations).

It has been previously demonstrated that tissue electroporation can be modeled as a conductivity (σ) change due to the tissue permeabilization (Sel et al. 2005). Accordingly, in our numerical models we took into consideration the mathematical relationship between the skin and muscle conductivities and the local electric field intensity in the following manner: a magnitude of E below the reversible threshold E_{rev} does not permeabilize the cell membranes, and therefore, no changes in conductivity are expected (σ is constant); when the local electric field intensity exceeds the E_{rev} threshold, the cell membrane is electropermeabilized and tissue conductivity increases according to the function $\sigma(E)$. In order to numerically study the electroporation process in a complete model that is composed of different tissues, the electroporation parameters σ_0, σ_1, E_{rev}, E_{irrev} and $\sigma(E)$ between the thresholds need to be determined in each of the single tissues separately, as previously demonstrated by Pavselj et al. (2005). Similarly, in order to numerically study the electroporation of muscle tissue electropulsed transcutaneously, we first built single models of skinfolds (Fig. 2) and muscle tissue (Fig. 3) separately and determined the corresponding electroporation parameters based on the analysis of a permeabilization sequence (Sel et al. 2005). The electroporation parameters for each of the tissues were determined considering that the acceptation criterion was that the output of the models using these parameters are those that best fit the experimental data (i.e., the electroporation parameters were varied until good agreement between the computed and measured current–voltage $I(U)$ relationship was obtained). We found that the $\sigma(E)$ function in the skinfold model was an exponential one (Eq. 6 with $B = 50{,}000$), while in the skeletal muscle model the function $\sigma(E)$ was sigmoid (Eq. 7 with $B = 10{,}000$). The electroporation parameters calculated for each of the tissues are listed in Table 1. The $\sigma(E)$ was chosen so that parameters such as E_{rev}, E_{irrev}, σ_o and σ_1 were as close as possible to the experimentally determined values. By varying all the functions of $\sigma(E)$, we noticed that $\sigma(E)$ can also be described with all the functions through proper adjustment of the electroporation parameters, which may be too far from the biologically justifiable values determined in the experiments, as previously suggested by Pavselj et al. (2005).

Different functions of $\sigma(E)$ are needed to describe the distribution of tissue electroporation in our models of muscle and skin tissue. This is probably due to differences in biological properties (i.e., cell size and distribution, electrical properties of intra- and extracellular media) of the tissues analyzed.

The $\sigma(E)$ functions with E_{rev} and E_{irrev} found in single models of skin (Fig. 2) and muscle (Fig. 3) were applied to the individual skin and muscle models composing the complete muscle model (Fig. 4). The same values of voltages of transcutaneous muscle electroporation in vivo (Fig. 1d) were applied to the contact surfaces of the complete muscle model (Fig. 4). In order to fine-tune the complete muscle model for the transcutaneously electroporated muscle in vivo, we also varied the thickness of the skin (d_{skin} parameter in Fig. 4) until the $I(U)$ relationship matched the measured one.

In our model of muscle with skin the skin layer takes into account the complex skin layer tissue. In the literature adult rat skin thickness was determined to be around 1 mm (Ngawhirunpat et al. 2002). However, our first calculations were made with a model in which the skin layer thickness was 0.5 mm. We changed the thickness of the skin layer from 0.5 to 1.4 mm. The calculations showed that in our models the smaller the thickness of the skin (i.e., lower resistance), the higher the electric current calculated. A skin thickness of 1.4 mm resulted in the best agreement between the measured and calculated currents, which was a very positive result since the thickness of the skinfold (two times the complex skin layer) of the same animals treated in the experiments was 2.8 mm (Fig.1b).

Since electric current gives quantitative information about tissue geometry and electric properties (i.e., tissue conductivity changes), good agreement between calculated and measured electric current at the end of electroporation

for the corresponding applied voltages validated our 3D finite element models. The agreement between calculated and measured current–voltage relationships obtained for the skinfold analysis is shown in Fig. 6a. The comparison of agreements between calculated and measured current–voltage relationships obtained for muscle and muscle with skin is shown in Fig. 6b.

At the lowest voltages the slope of the $I(U)$ curve is low and linear, meaning that electroporation does not yet occur. The value of U at which the $I(U)$ relationship starts to diverge from its linear curve indicates that the reversible threshold value of the local electric field for tissue electroporation has been obtained. The threshold value E_{rev} in the directly electroporated muscle model was obtained at $U = 136$ V and in the muscle model electroporated transcutaneously at $U = 252$ V. The local electric field distribution in both muscle models is displayed in Fig. 7 in the xy cross-sectional plane located in the middle of the two plate electrodes. To more precisely analyze the local electric field distribution around the reversible threshold obtained with the sequence analysis ($E_{rev} = 240$ V/cm), we visualized E in the range 0–250 V/cm for the first four applied voltages. The reversible threshold for muscle electroporation is obtained at a lower value of applied voltage ($U = 136$ V) in the model of directly electroporated muscle (Fig. 7a) than in the model of muscle electroporated through the skin ($U = 252$ V) (Fig. 7b) due to the high resistance of the skin layer that must be overcome

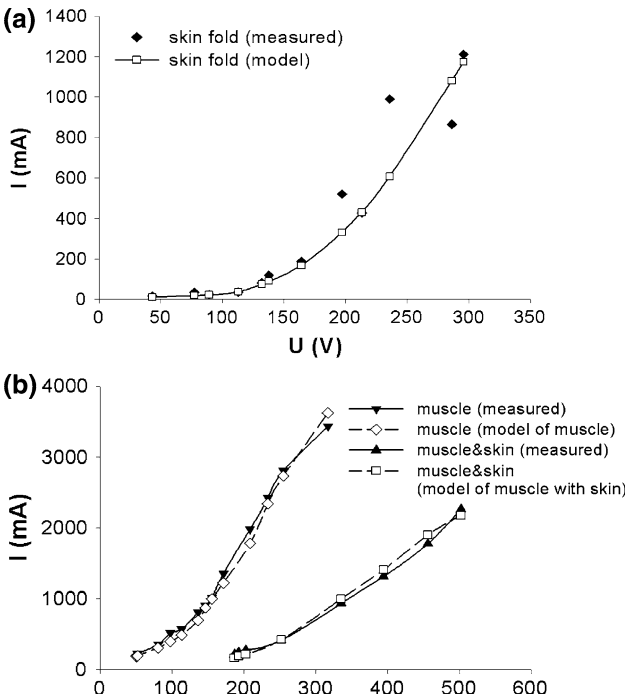

Fig. 6 Calculated and in vivo measured current–voltage relationships for **a** skinfold and **b** muscle and muscle with skin

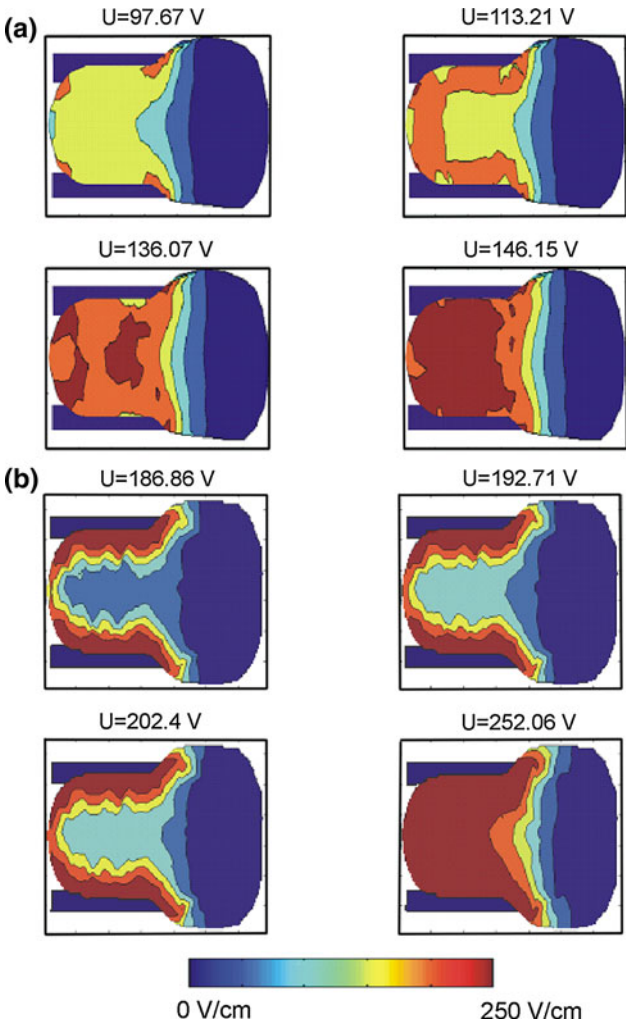

Fig. 7 Distribution of E in the model of muscle alone (**a**) and in the muscle model with skin (**b**)

by a higher U in order to target the underlying muscle tissue with $E > E_{rev}$. In other words, the reversible threshold value in muscle with skin was obtained at a higher U because the skin tissue needed to be permeabilized first. Namely, when U is applied, the electric field is distributed within the complex tissue according to its specific electric properties (acting as a voltage divider), meaning that the electric field is highest in the layer with the highest electric resistivity (i.e., lowest conductivity) (Pavselj and Miklavcic 2008). When the skin becomes permeabilized, its conductivity increases according to the function $\sigma(E)$, which leads to electric field redistribution in the skin and its underlying more conductive tissues (in our case muscle tissue), as shown in Fig. 7b. If U is too low, the highest electric field remains in the skin layer and does not reach the muscle.

Nonuniform distribution of tissue permeabilization also occurs in a single tissue (in our case muscle tissue) due to

an inhomogeneous E distribution. The increase in tissue conductivity, and thus tissue permeabilization, first occurs in close proximity to the electrodes (i.e., the region with the highest E). The conductivity increase causes a modification in E distribution according to $\sigma(E)$, which consequently causes another change in tissue conductivity and the distribution of muscle permeabilization away from the electrodes, toward the regions with lower initial E between the electrodes, as shown in Fig. 7a.

In most of the studies on skin electroporation (Prausnitz et al. 1993; Pliquett et al. 1995), a pronounced change in skin resistance was observed above 50 V for the experiments done through a single skin tissue layer. In order to compare our analysis on changes in electric properties in the skin layer in the complete muscle model to the data from the literature, we also calculated the resistance of the complete muscle model for each of the voltages applied as well as a few additional voltages ($U < 186.86$ V) that were not applied during in vivo experiments. The calculated resistance–voltage relationship, $R(U)$, is shown in Fig. 8. From the $R(U)$ curve it can be observed that a visible drop in skin resistance was obtained at $U > 100$ V, which is in agreement with the abovementioned studies, proved in our study by electroporation of the double skin layer. The increase in skin conductivity, thus the drop in skin resistance, in our skinfold (double skin layer) model was also observed at $U > 100$ V, as shown in Fig. 6a. In a similar experimental and numerical study on cutaneous tumor electroporation, pronounced changes in skin conductivity were also observed at 100 V of applied voltage (Pavselj et al. 2005). Therefore, the conductivity change and the geometry of the skin layer numerically found in our complete muscle model are in agreement with previous studies on skin.

In order to analyze the influence of the skin layer on muscle electroporation, we used in vivo experimental data of ^{51}Cr-EDTA uptake measured in muscle electroporated directly and transcutaneously. The ^{51}Cr-EDTA molecules from the extracellular compartments could enter only the electroporated cells. Both measurements were done at the same applied voltages as in the total current measurement in vivo. The experimentally obtained ^{51}Cr-EDTA (U/d) relationships for muscle electroporated directly and transcutaneously are shown in Fig. 9a. The start of the ^{51}Cr-EDTA-uptake increase should correspond to the start of reversible electroporation, the start of ^{51}Cr-EDTA-uptake decline should correspond to the point of irreversible electroporation.

We then analyzed the electroporation parameters of muscles electroporated directly and transcutaneously by comparing the local electric field distribution in the model of muscle without skin (Fig. 3) with the local electric field distribution obtained only in the muscle inside the

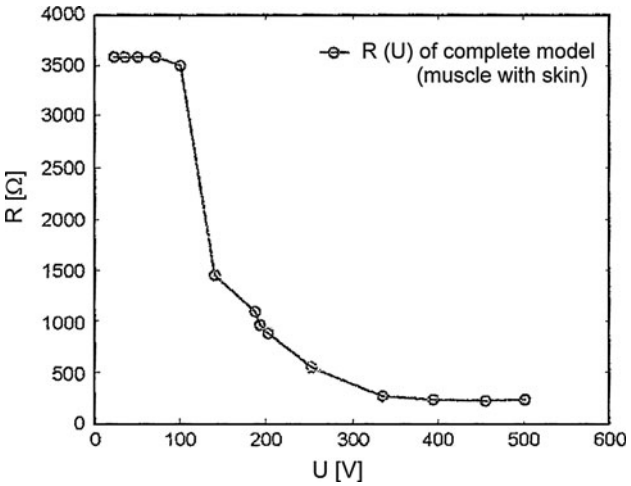

Fig. 8 Calculated resistance–voltage relationship for the complete model from Fig. 4 (muscle with skin)

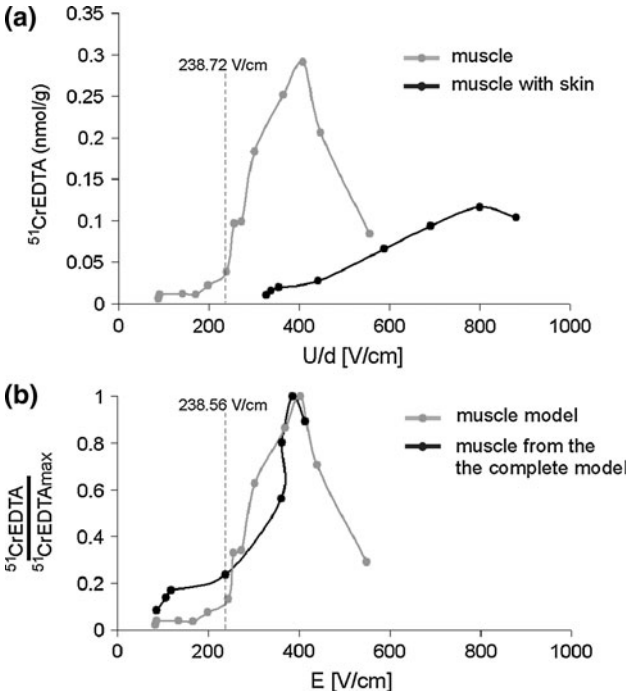

Fig. 9 **a** Measured ^{51}CrEDTA uptake (nmol/g) in muscle electroporated directly and transcutaneously (the skin is present) and **b** ^{51}CrEDTA uptake in muscle models electroporated directly and transcutaneously (skin is numerically removed from complete model). For muscle from the complete model we took into account the ^{51}CrEDTA uptake from the muscle with skin (**a**) and normalized the ^{51}CrEDTA-uptake values for both muscles (with and without skin) to the maximum uptake obtained in the directly electroporated muscle (^{51}CrEDTAmax = 0.29 nmol/g, as shown in **a**). (U values in **a** are normalized to the interelectrode distance ratio (U/d). The interelectrode distance used in all experiments was $d = 5.7$ mm. The E in **b** is the average local electric field calculated in the model of muscle electroporated directly and in the model of muscle from the complete model without skin [i.e., with skin numerically removed])

complete muscle model with skin (Fig. 4). The local electric field was analyzed at the end of the electroporation process (i.e., at the end of the sequence analysis). Namely, the average electric field intensities were calculated in the space between the two plate electrodes (the regions between electrodes marked with the dashed square in Figs. 3, 4), where the electric field was the most homogeneous (i.e., where the electric field approaches U/d). In this way we numerically removed the skin layer from the complete muscle model with skin shown in Fig. 4. The numerical results of E in the muscle from the complete model were then compared to the average E in the muscle electroporated directly, as shown in Fig. 9b. The maximum uptake of ^{51}CrEDTA in transcutaneously electroporated muscle was obtained at higher voltage applied compared to the maximum uptake obtained in directly electroporated muscle: 0.12 nmol/g ($U = 233$ V, $U/d = 409$ V/cm) versus 0.29 nmol/g ($U = 456$ V, $U/d = 800$ V/cm) (Fig. 9a). When we calculated the local electric field in the muscle models and numerically removed the skin from the complete model, we showed that uptake of ^{51}CrEDTA in muscle that was electroporated through the skin occurred at similar local electric fields as the uptake of ^{51}CrEDTA in directly electroporated muscle (Fig. 9b). The maximum uptakes in the muscle from the complete model (0.12 nmol/g) and the model of directly electroporated muscle (0.29 nmol/g) were obtained at $E = 386$ and 403 V/cm, respectively (Fig. 9b). In Fig. 9b the comparison of ^{51}CrEDTA uptake in both muscle models (directly electroporated muscle and the complete model of muscle with skin removed) is given for the ^{51}CrEDTA values normalized to the maximum uptake ^{51}CrEDTAmax obtained in the directly electroporated muscle (^{51}CrEDTAmax = 0.29 nmol/g).

The average value of E in the model of muscle alone calculated at $U = 136$ V ($U/d = 238.72$ V/cm) was $E_{rev} = 242$ V/cm, whereas the average E in muscle in the complete model with skin at the higher applied voltage $U = 252$ V ($U/d = 442$ V/cm) was calculated to be almost the same as in muscle without skin, $E_{rev} = 238.56$ V/cm, as shown in Fig. 9b. Similarly, the irreversible threshold values calculated as average local E for muscle alone and muscle with skin were $E_{irrev} = 443$ V/cm (at applied $U = 255$ V, $U/d = 447$ V/cm) and 414 V/cm (at applied $U = 502$ V, $U/d = 880$ V/cm), respectively. Based on these calculations, we conclude that the skin layer has, as expected, no influence on the thresholds of the local electric field needed to successfully electroporate muscle tissue. We did, however, find that the presence of skin affects ^{51}CrEDTA uptake into the muscle while being electroporated through the skin, which can be explained by the dependence of the electroporation level on the duration and the number of electroporation pulses. Namely, due to the presence of the skin, the effective duration of the electroporation pulses can be shorter, which consequently results in a lower ^{51}Cr-EDTA uptake in the muscle tissue (the maximum uptake of ^{51}CrEDTA in transcutaneously electroporated muscle was by a factor of 2.41 lower compared to the maximum uptake in directly muscle electroporated muscle, Fig. 9). It is well known that the molecular flux through the permeabilized membrane depends on the duration and number of electroporation pulses (Puc et al. 2003; Pucihar et al. 2008).

The threshold values calculated in both the model of muscle alone and the complete model with skin are similar to the threshold values obtained with sequence analysis in the model of muscle alone, $E_{rev} = 240$ and 450 V/cm, respectively. From Fig. 9 it can be seen that in muscle electroporated directly the average local electric field in the region between the electrodes (gray curve in Fig. 9b), where the tissue is (region marked with dashed square in Fig. 3), is almost equal to the voltage over the interelectrode distance ratio, U/d (gray curve in Fig. 9a), and is thus almost homogeneous. Consequently, the error we make using U/d values to approximately determine the threshold value of local electric field to successfully electroporate muscle without skin is acceptably small. However, for the precise determination of the local electric field threshold value needed for the electroporation of muscle inside a complex tissue, a realistic numerical model that takes into account realistic geometries, electric properties and electric field nonhomogeneities due to the tissue permeabilization of all the composing tissues needs to be used in combination with corresponding in vivo experiments.

Our results are comparable with data obtained in a similar numerical and in vivo study for the same type of pulses as those used in our study (eight pulses, 100 μs, 1 Hz) (Pavselj et al. 2005), where the E_{rev} and E_{irrev} for muscle electroporated directly were estimated to be 200 and 450 V/cm, respectively. In another study (Gehl et al. 1999), the combination of in vivo experiments (transcutaneous muscle electroporation using plate electrodes with $d = 4$ mm) and 2D numerical models resulted in a higher electroporation threshold (450 V/cm) compared to the one obtained in our study ($E_{rev} = 238$ V/cm) since in their study the tissue between electrodes was considered homogeneous in two dimensions, meaning that differences in skin and muscle electric conductivity and geometry were not taken into account.

A similar reversible electroporation threshold ($E_{rev} = 200$ V/cm) for muscle without skin and for the same orientation (perpendicular) of the applied electric field with respect to the muscle fibers was found in our previous study where thresholds in the two main muscle orientations (electrodes parallel or perpendicular to the main muscle fiber axes) were compared (Corovic et al. 2010).

Conclusion

In this study we present realistic numerical models of electroporated skinfold and skeletal muscle tissue electroporated directly and transcutaneously, which we developed in order to analyze the electroporation process in skin and muscle tissues in vivo. The models were developed by validating numerical calculations on in vivo experimental results. We determined how to map electropermeabilization by identifying the local electric field distribution in skin and muscle tissues. Namely, we found the functional dependence of tissue conductivity on electric field intensity, $\sigma(E)$, to be exponential for skin with electroporation thresholds $E_{rev} = 480$ V/cm and $E_{irrev} = 1{,}050$ V/cm and sigmoid for muscle tissue with $E_{rev} = 240$ V/cm and $E_{irrev} = 430$ V/cm. The same electroporation threshold values, E_{rev} and E_{irrev}, were found for both muscles electroporated directly and transcutaneously. We thus conclude that the skin layer has, as expected, no influence on the thresholds of the local electric field intensity needed for successful muscle tissue electroporation, but it does require higher voltage to be applied between the electrodes when muscle is electroporated transcutaneously. Our model of muscle with skin also confirms the in vivo findings of previous studies that electroporation "breaks" the skin barrier when the applied voltage is above 50 V.

We also showed that the error of an approximate estimation of electroporation threshold values in in vivo experiments by calculating the U/d ratio, without numerical calculations of local electric field distribution, is small enough only if the plate electrodes are used and only for one type of tissue placed between the electrodes. For more complex tissues with different geometric and electrical properties, a combination of realistic numerical modeling and in vivo experiments needs to be used for the precise determination of electroporation threshold values.

It is also important to note that the thresholds of the local electric field for tissue electroporation depend on the type of molecules used for the detection of in vivo tissue permeabilization (Kotnik et al. 2000) and electroporation pulse characteristics (i.e., duration and number of pulses as well as pulse repetition frequency). Thus, the threshold values determined in our study are relevant for the setting of eight pulses of 100-μs duration at a repetition frequency of 1 Hz. For the precise electroporation threshold determination for other pulse parameters, our numerical models remain valid, but additional in vivo experiments need to be done and the results included in the models.

The findings of our study carry important practical information for treatment planning in electroporation-mediated therapies such as gene electrotransfer into muscle, transdermal drug and gene delivery and clinical electrochemotherapy.

Acknowledgments This research was supported in part by the European Commission under the fifth framework (Grant Cliniporator QLK3-1999-00484), Slovenian Research Agency, CNRS (Centre National de la Recherche Scientifique), Institute Gustave-Roussy and Ad-Futura. This research was conducted in the scope of LEA EBAM. The authors thank Dr. David Cukjati and Dr. Danute Batiuskaite for the results of in vivo experiments performed in the lab of L. M. M. (Institut Gustave-Roussy, Villejuif, France) as well as Derek Snyder for help in proofreading and editing the text.

References

Breton M, Mir LM (2011) Microsecond and nanosecond electric pulses in cancer treatments. Bioelectromagnetics. doi:10.1002/bem.20692

Corovic S, Zupanic A, Miklavcic D (2008) Numerical modeling and optimization of electric field distribution in subcutaneous tumor treated with electrochemotherapy using needle electrodes. IEEE Trans Plasma Sci 36:1665–1672

Corovic S, Zupanic A, Kranjc S, Al Sakere B, Leroy-Willig A, Mir LM, Miklavcic D (2010) Influence of skeletal muscle anisotropy on electroporation: in vivo study and numerical modeling. Med Biol Eng Comput 48:637–648

Cukjati D, Batiuskaite D, André F, Miklavcic D, Mir LM (2007) Real time electroporation control for accurate and safe in vivo non-viral gene therapy. Bioelectrochemistry 70:501–507

Davalos R, Rubinsky B, Otten DM (2002) A feasibility study for electrical impedance tomography as a means to monitor tissue electroporation for molecular medicine. IEEE Trans Biomed Eng 49:400–403

Davalos RV, Otten DM, Mir LM, Rubinsky B (2004) Electrical impedance tomography for imaging tissue electroporation. IEEE Trans Biomed Eng 51:761–767

Denet AR, Vanbever R, Préat V (2004) Skin electroporation for transdermal and topical delivery. Adv Drug Deliv Rev 56:659–674

Edhemovic I, Gadzijev EM, Brecelj E, Miklavcic D, Kos B, Zupanic A, Mali B, Jarm T, Pavliha D, Marcan M, Gasljevic G, Gorjup V, Music M, Pecnik Vavpotic T, Cemažar M, Snoj M, Sersa G (2011) Electrochemotherapy: a new technological approach in treatment of metastases in the liver. Technol Cancer Res Treat 10:475–485

Gehl J, Mir LM (1999) Determination of optimal parameters for in vivo gene transfer by electroporation, using a rapid in vivo test for cell permeabilization. Biochem Biophys Res Commun 261:377–380

Gehl J, Sorensen TH, Nielsen K, Raskmark P, Nielsen SL, Skovsgaard T, Mir LM (1999) In vivo electroporation of skeletal muscle: threshold, efficacy and relation to electric field distribution. Biochim Biophys Acta 1428:233–240

Hojman P, Eriksen J, Gehl J (2009) In vivo imaging of far-red fluorescent proteins after DNA electrotransfer to muscle tissue. Biol Proc Online 11:253–262

Ivorra A, Al-Sakere B, Rubinsky B, Mir LM (2009) In vivo electrical conductivity measurements during and after electroporation of sarcomas: conductivity changes reflect treatment outcome. Phys Med Biol 54:5949–5963

Kos B, Zupanic A, Kotnik T, Snoj M, Sersa G, Miklavcic D (2010) Robustness of treatment planning for electrochemotherapy of deep-seated tumors. J Membr Biol 236:147–153

Kotnik T, Macek-Lebar A, Miklavcic D, Mir LM (2000) Evaluation of cell membrane electropermeabilization by means of non-permeant cytotoxic agent. Biotechniques 28:921–926

Mali B, Jarm T, Corovic S, Paulin-Kosir MS, Cemazar M, Sersa G, Miklavcic D (2008) The effect of electroporation pulses on functioning of the heart. Med Biol Eng Comput 46:745–757

Marty M, Sersa G, Garbay JR, Gehl J, Collins CG, Snoj M, Billard V, Geertsen PF, Larkin JO, Miklavcic D, Pavlovic I, Paulin-Kosir SM, Cemazar M, Morsli N, Soden DM, Rudolf Z, Robert C, O'Sullivan GC, Mir LM (2006) Electrochemotherapy—an easy, highly effective and safe treatment of cutaneous and subcutaneous metastases: results of ESOPE (European Standard Operating Procedures of Electrochemotherapy) study. Eur J Cancer Suppl 4:3–13

Mathiesen I (1999) Electropermeabilisation of skeletal muscle enhances gene electrotransfer in vivo. Gene Ther 6:508–514

Miklavcic D, Beravs K, Semrov D, Cemazar M, Demsar F, Sersa G (1998) The importance of electric field distribution for effective in vivo electroporation of tissues. Biophys J 74:2152–2158

Miklavcic D, Semrov D, Mekid H, Mir LM (2000) A validated model of in vivo electric field distribution in tissues for electrochemotherapy and for DNA electrotransfer for gene therapy. Biochim Biophys Acta 1523:73–83

Miklavcic D, Pavselj N, Hart FX (2006) Electric properties of tissues. In: Wiley encyclopedia of biomedical engineering. Wiley, New York

Mir LM, Orlowski S, Belehradek J Jr, Teissié J, Rols MP, Sersa G, Miklavcic D, Gilbert R, Heller R (1995) Biomedical applications of electric pulses with special emphasis on antitumor electrochemotherapy. Bioelectrochemistry 38:203–207

Mir LM, Bureau MF, Gehl J, Rangara R, Rouy D, Caillaud JM, Delaere P, Branellec D, Schwartz B, Scherman D (1999) High-efficiency gene transfer into skeletal muscle mediated by electric pulses. Proc Natl Acad Sci U S A 74:4262–4267

Ngawhirunpat T, Hatanaka T, Katayama K, Yoshikawa H, Kawakami J, Adachi I (2002) Changes in electrophysiological properties of rat skin with age. Biol Pharm Bull 25:1192–1196

Pavlin M, Miklavcic D (2003) Effective conductivity of a suspension of permeabilized cells: a theoretical analysis. Biophys J 85: 719–729

Pavlin M, Pavselj N, Miklavcic D (2002) Dependence of induced transmembrane potential on cell density, arrangement, and cell position inside a cell system. IEEE Trans Biomed Eng 49: 605–612

Pavselj N, Miklavcic D (2008) Numerical modeling in electroporation-based biomedical applications. Radiol Oncol 42:159–168

Pavselj N, Bregar Z, Cukjati D, Batiuskaite D, Mir LM, Miklavcic D (2005) The course of tissue permeabilization studied on a mathematical model of a subcutaneous tumor in small animals. IEEE Trans Biomed Eng 52:1373–1381

Pliquett U, Langer R, Weaver JC (1995) Changes in the passive electrical properties of human stratum corneum due to electroporation. BBA 1239:111–121

Prausnitz MR, Bose VG, Langer R, Weaver JC (1993) Electroporation of mammalian skin: a mechanism to enhance transdermal drug delivery. Proc Natl Acad Sci U S A 90:10504–10508

Prud'homme GJ, Glinka Y, Khan AS, Draghia-Akli R (2006) Electroporation enhanced nonviral gene transfer for the prevention or treatment of immunological, endocrine and neoplastic diseases. Curr Gene Ther 6:243–273

Puc M, Kotnik T, Mir LM, Miklavcic D (2003) Quantitative model of small molecules uptake after in vitro cell electropermeabilization. Bioelectrochemistry 60:1–10

Pucihar G, Kotnik T, Miklavčič D, Teissié J (2008) Kinetics of transmembrane transport of small molecules into electropermeabilized cells. Biophys J 95:2837–2848

Sel D, Cukjati D, Batiuskaite D, Slivnik T, Mir LM, Miklavcic D (2005) Sequential finite element model of tissue electropermeabilization. IEEE Trans Biomed Eng 52:816–827

Tevz G, Pavlin D, Kamensek U, Kranjc S, Mesojednik S, Coer A, Sersa G, Cemazar M (2008) Gene electrotransfer into murine skeletal muscle: a systematic analysis of parameters for long-term gene expression. Technol Cancer Res Treat 7(2):91–154

UKCCCR (1998) UKCCR guidelines for welfare of animals in experimental neoplasia (second edition). Br J Cancer 77:1–10

Valic B, Golzio M, Pavlin M, Schatz A, Faurie C, Gabriel B, Teissie J, Rols MP, Miklavcic D (2003) Effect of electric field induced transmembrane potential on spheroidal cells: theory and experiments. Eur Biophys J 32:519–528

Zupanic A, Ribaric S, Miklavcic D (2007) Increasing the repetition frequency of electric pulse delivery reduces unpleasant sensations that occur in electrochemotherapy. Neoplasma 54:246–250

Zupanic A, Corovic S, Miklavcic D (2008) Optimization of electrode position and electric pulse amplitude in electrochemotherapy. Radiol Oncol 42:93–101